Chemical Engineering Science 171 (2017) 233–243

Contents lists available at ScienceDirect

Chemical Engineering Science

journal homepage: www.elsevier.com/locate/ces

Continuous synthesis of PVP stabilized biocompatible gold nanoparticles with a controlled size using a 3D glass capillary microfluidic device

Monalie V. Bandulasena, Goran T. Vladisavljević *, Omololu G. Odunmbaku, Brahim Benyahia *

Loughborough University, Chemical Engineering Department, Epinal Way, Loughborough, Leicestershire LE11 3TU, United Kingdom

HIGHLIGHTS

- Continuous synthesis of AuNPs in co-flow glass capillary microfluidics was achieved.
- Impact of device geometry and reactant conditions on size & PDI was investigated.
- Stabilization of AuNPs using PVP with different molecular weights was investigated.
- Reactor fouling was mitigated using PVP & ascorbic acid solution with higher pH.
- Enhanced control of size & PDI of AuNPs achieved by optimising reaction conditions.

GRAPHICAL ABSTRACT

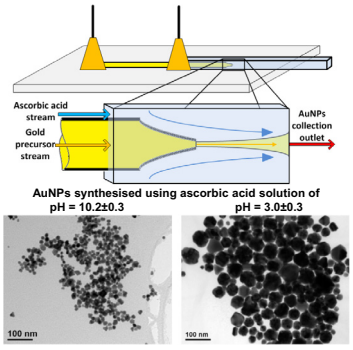

ARTICLE INFO

Article history:
Received 31 January 2017
Received in revised form 16 May 2017
Accepted 20 May 2017
Available online 25 May 2017

Keywords:
Gold nanoparticles
Glass capillary microfluidics
Continuous production
Ascorbic acid
Polyvinylpyrrolidone
Microfluidic micro-mixing

ABSTRACT

A reliable glass capillary microfluidic method was developed for a continuous production of well-controlled gold nanoparticles (AuNPs) capped with polyvinylpyrrolidone (PVP) of different molecular weights (PVP K15, PVP K30 and PVP K90). A two-phase co-flow glass capillary microfluidic device with an injection orifice diameter ranging between 100 and 240 μm was used to synthesise 100–240 μm was used to synthesise AuNPs via the chemical reduction between tetrachloroaurate trihydrate ($HAuCl_4{\cdot}3H_2O$) and ascorbic acid. AuNPs with an average diameter between 48 and 135 nm were synthesised, as determined by DLS measurements. Decreasing the injection orifice diameter, increasing the flow rate of ascorbic acid stream and its pH resulted in smaller AuNPs. The polydispersity index (PDI) was found to be independent on the injection orifice diameter or the molecular weight of PVP, but increased with the increase of flow rate and the pH of ascorbic acid stream. The stability study over 6-week period confirmed that PVP K30 with an average M_w of 40000 g/mol was the best capping agent to synthesize and stabilise smaller AuNPs. The reactor fouling due to deposition of AuNPs on reactor walls and orifices was mitigated by hydrophobization of reactor/capillary walls with octadecyltrimethoxisilane and the use of ascorbic acid solution of higher pH.

1. Introduction

Gold nanoparticles (AuNPs) also known as colloidal gold or soluble gold have been used in day to day human life for more than 2500 years as a remedy to venereal diseases, dysentery, epilepsy and tumors, as a medical diagnostic tool (Horikoshi and Serpone,

* Corresponding authors.
E-mail addresses: G.Vladisavljevic@lboro.ac.uk (G.T. Vladisavljević), B.Benyahia@lboro.ac.uk (B. Benyahia).

http://dx.doi.org/10.1016/j.ces.2017.05.035
0009-2509/

2013) and for decorative purposes. The Lycurgus Cup, which reflects light differently when illuminated from inside and outside, possesses this property thanks to the AuNPs embedded in the dichroic glass used to make the cup (Perks, 2010).

AuNPs exhibit interesting surface and quantum properties such as surface plasmon resonance and size-dependent optical, chemical, physical and electromagnetic properties, which differ from those of bulk gold (Roduner, 2006). As a result, AuNPs still attract considerable interest in drug and gene delivery (Pissuwan et al., 2011), imaging and radiotherapy (Conde et al., 2012), treatments of cancer and cardiovascular diseases (Spivak et al., 2013), biosensing and pathogen detection (Verma et al., 2015), fabrication of nonvolatile memory devices (Lee, 2010) and catalysts (Qureshi et al., 2016).

AuNPs are typically synthesized using the redox reaction between a suitable gold salt and a reducing agent such as sodium citrate, sodium borohydride ($NaBH_4$), and ascorbic acid (Turkevich et al., 1951; Wagner and Kohler, 2005). Green and ecofriendly reducing agents such as citrus fruit juices, and plant and algal extracts have also been investigated (Chandran et al., 2006; Gao et al., 2014; Nune et al., 2009; Rajeshkumar et al., 2013). Ascorbic acid is a cheap, nontoxic, biocompatible, and relatively weak reducing agent that can produce AuNPs with a size between 7 and 25 nm at the room temperature (Jun et al., 2012). $NaBH_4$ is one of the strongest reducing agents which can be used to synthesise smaller particles than ascorbic acid. However, $NaBH_4$ reacts with water and generates hydrogen, which forms bubbles in the microfluidic channels that interfere with the flow pattern and interrupt or affect the continuous production of AuNPs and inherently their properties.

According to the classical nucleation theory (CNT), the formation of NPs follows two major steps: nucleation and then particle growth, which are both triggered by mixing of reactants. The rate and efficiency of mixing determines the size and the size distribution of the synthesised NPs (Sugano et al., 2010; Thanh et al., 2014). Compared to bulk and batch methods, continuous microfluidic devices offer an enhanced control over mixing, which in-turn enables a better control of both nucleation and growth and consequently, in agreement with the classical nucleation theory, the size distribution of the synthesized NPs can be precisely tuned. Due to the laminar flow that takes place inside micro-channels, controlled hydrodynamic conditions are quickly established and maintained throughout the production process. As such, better control of reaction time, mixing, heat and mass transfer can be achieved leading to a better control of the particle size and the size distribution (Lazarus et al., 2012). Although microfluidic devices produce very small amount of products due to the limited reactor size and small flow rates, they are versatile in terms of applications, device geometries, flow features (e.g. co-flow, flow focussing and droplet generation). In addition, they are more economic and safe, as they require a smaller amount of expensive or eventually toxic chemicals (Zhao et al., 2011), and proven to be excellent candidates for the integrated continuous flow manufacturing (Heider et al., 2014; Mascia et al., 2013). Moreover, microfluidic devices enable easy manipulation of the operating conditions while production is running, which makes it possible to run a set of experiments in one go.

Over the last decade, AuNPs were synthesized using different types of microfluidics. Wagner et al. (2004) are the first to report the use of single phase reaction system to produce AuNPs in a microfluidic device made by anodic bonding of wet-etched Pyrex glass and silicon. Duraiswamy and Khan (2009) used a PDMS microfluidic device with segmented flow to synthesize anisotropic AuNPs using the seeded growth method. Lazarus et al. (2012) used a multiple inlet T-junction PDMS device to synthesize AuNPs within ionic liquid drops. Gomez et al. (2014) synthesised hollow AuNPs in a millifluidic device made out of coiled PTFE tubing using $NaBH_4$ as a reducing agent and cobalt as a sacrificial template. Gomez-de Pedro at al. (2010) used a microfluidic system based on the low-temperature co-fired ceramics technology to synthesise functionalised AuNPs using $NaBH_4$ reduction method.

In this work, polyvinylpyrrolidone (PVP) capped AuNPs were synthesized in a continuous co-flow microfluidic device made out of coaxially aligned borosilicate glass capillaries, using ascorbic acid as the reducing agent and tetrachloroaurate(III) ions as the gold precursor. Glass capillary devices are less difficult to fabricate and cheaper than PDMS devices which require processes such as photolithography, etching and moulding. Another advantage of glass capillary over PDMS devices lies in the ability of achieving an axisymmetric (3D) flow geometry inside the device. Most PDMS channels have 2D flow geometries, which promote fouling and deposition of the particles onto reactor walls (Othman et al., 2015a). Borosilicate glass is inert with respect to most of the solvents and can withstand relatively higher pressures as it has high Young's modulus. A such, the glass capillary is not subject to significant deformation or shape / geometry modification during operation, which ensures consistent operating conditions, as opposed to most of the polymers used for microfabrication, including PDMS (Bouras et al., 2009; Johnston et al., 2014). In addition, Borosilicate glass has excellent optical transparency, which enables visual in-situ control and adjustment of the flow rates without interruption of the production process. Borosilicate glass capillary devices were used for reproducible synthesis of biodegradable polymeric NPs (Othman et al., 2015a,b), drug nanocrystals (Odetade and Vladisavljević, 2016), liposomes (Vladisavljević et al., 2014a), polymeric micelles (Laouini et al., 2013), polylactic acid and polycaprolactone microparticles (Vladisavljević et al., 2014a,b; Ekanem et al., 2015) and emulsions (Nabavi et al., 2015). To the best of our knowledge, this is the first application of glass capillary microfluidic devices for the synthesis of size-tailored AuNPs. The effect of operating and geometrical parameters on the size and polydispersity of the produced AuNPs has been investigated, such as orifice diameter of the injection capillary, pH of the ascorbic acid stream, flow rates of the reactant streams, and the type of capping agent.

2. Materials and methods

2.1. Materials

Hydrogen tetrachloroaurate(III) ($HAuCl_4 \cdot 3H_2O$) (≥99.9% trace metals basis) and reagent grade crystalline L-ascorbic acid were supplied from Sigma Aldrich, UK. The gold precursor stream was 1 mM aqueous $HAuCl_4$ solution containing 1% (w/v) polyvinylpyrrolidone (PVP) of different molar masses (PVP K15 with $M_w \sim 10{,}000$ g/mol, PVP K30 with $M_w \sim 40{,}000$ g/mol and PVP K90 with $M_w \sim 360{,}000$ g/mol, Sigma Aldrich, UK) as the capping agent. The reducing agent stream was 20 mM aqueous ascorbic acid solution with two different pH values (3.0 ± 0.3 and 10.2 ± 0.3) adjusted using 2 M NaOH solution (Fisher Scientific, UK). A Jenway 3340 Ion Meter (Keison, UK) was used to monitor the pH. Octadecyltrimethoxisilane (OTMS) (Sigma Aldrich, UK) was used for hydrophobic treatment of the square capillary. Reagent grade acetone (Fisher Scientific, UK) was used for cleaning purposes. Aqua regia (a mixture of HNO_3 and HCl prepared by mixing 2 ml of 36% HNO_3 and 8 ml of 70% HCl) was used to clean all the glassware prior to the experiments. Milli-Q water was used to prepare all aqueous solutions.

2.2. Device fabrication and experimental procedure

The microfluidic device was fabricated using two borosilicate capillary tubes, a round tube with 1.0 mm O.D. and 0.58 mm I.D.

(Intracel Ltd, UK) and a square tube with an inner diameter of 1.05 ± 0.1 mm and a wall thickness of 0.2 mm (Atlantic International Technologies, USA). The inner capillary was heated and pulled using the P-97 Flaming/Brown micropipette puller (Sutter Instrument Company, USA) to produce a 20 μm tip. By using the Narishige's MF-830 microforge (Linton Instrumentation, UK) and grazing the tip against abrasive paper, a tapered end of the capillary was adjusted to the desired inner diameter (D_o) of 100, 180 or 240 μm and treated with OTMS and render it hydrophobic. To investigate the effect of hydrophobic treatment on the size of the synthesised NPs, the inner walls of the square capillary were silanised by soaking the capillary in a 20% HCl solution in ethanol for 30 min and then in an OTMS solution for at least 15 h. The capillary was then rinsed with distilled water and dried. OTMS molecules attach to the glass surface via siloxane bond (≡Si-O-) formation, while long alkyl chains form a tightly packed hydrophobic monolayer.

38 × 75 mm Corning® microscope slide was used as a platform for the microfluidic device after being cleaned with deionised water and acetone. Devcon® 5 min two component epoxy glue (ITW Devcon, UK) was used to glue the square capillary onto the microscope slide, as shown in Fig. 1(b). After a drying period, the slide with the attached square capillary was placed under the XD63 inverted microscope (GX Microscopes, USA), which was attached to a Phantom V9.0 high speed camera (Vision Research, Ametek, USA). A surface treated round capillary was then partially inserted into the square capillary and aligned. Epoxy glue was applied to the exposed part of the round capillary to bond it to the microscope slide.

In the next step, two BD PrecisionGlide™ needles (2.5 mm O.D. and 0.9 mm I.D., Sigma Aldrich, UK) were placed on top of delivery points of the capillaries, as shown in Fig. 1(b) (allowing capillary openings to be placed inside the yellow plastic hub of the needles) and securely glued onto the microscopic slide. Fig. 1(a) depicts the schematic of the co-flow glass capillary microfluidic device.

Two 11 Elite syringe pumps (Harvard Apparatus, Cambridge, UK) were used to deliver the reactant streams at required flow rates from 10 ml SGE gas tight syringes. Fine bore Portex polyethylene medical tubing (0.86 mm I.D. and 1.52 mm O.D., Smiths Medicals, UK) was used to feed reactants and collect products to and from the microfluidic device. AuNPs were formed right after the orifice when both reactant streams were mixed in a laminar flow, as illustrated in Fig. 1(a). The process was observed and recorded using a Phantom V9.0 high speed camera at 25 frames per second with 576 × 288 resolution which was attached to the inverted microscope.

Table 1 summarizes the experimental conditions used to investigate the effect of different conditions and three different injection capillary orifice diameters (D_o) on the particle size (D_p), polydispersity index (PDI), and the absorbance spectrum of the synthesized AuNPs. PDI is a dimensionless measure of the broadness of the size distribution.

2.3. Characterisation of the AuNPs

2.3.1. Particle size and PDI analysis

The mean particle size and PDI were determined by dynamic light scattering (DLS) using a Delsa™ Nano HC particle size analyser (Beckman Coulter, UK). Approximately 3 ml of the prepared nanosuspension was transferred in a disposable polyethylene cuvette and placed into the analyser. The sample was illuminated by a laser beam and the fluctuations of the intensity of the scattered light, due to Brownian motion of the NPs, were measured at a scattering angle of 165° by a fast photon detector. Smaller NPs move faster than larger ones and therefore, the timescale of intensity fluctuations is shorter for smaller particles allowing the particle size distribution to be measured. The data acquisition time for each measurement was 120 s. The measurements were repeated 3 times for each sample and the mean particle size was reported.

2.3.2. UV–Vis spectroscopy

A Perkin Elmer Lambda 35 UV/VIS spectrometer was used to measure the absorbance spectra of the reactant and product solutions. Deuterium and Tungsten-halogen lamps were used to provide respectively UV and visible range of electromagnetic wavelengths. A polyethylene cuvette containing 3 ml of the product sample was placed inside the instrument beside the reference sample cuvette. Milli Q water was used as the reference sample as all the solutions were prepared using Milli Q water. A beam of incident light with a wavelength ranging from 300 to 800 nm was split into two equal beams that passed through the reference sample and the product sample. The absorbance spectrum of the product was determined by comparing the intensities of the two beams. AuNP suspensions appear in different colours due to their wavelength-dependent absorbance of light corresponding to their size and surface properties. As such, the size of the particles can be estimated from the UV–Vis absorption spectrum (Verma et al., 2014).

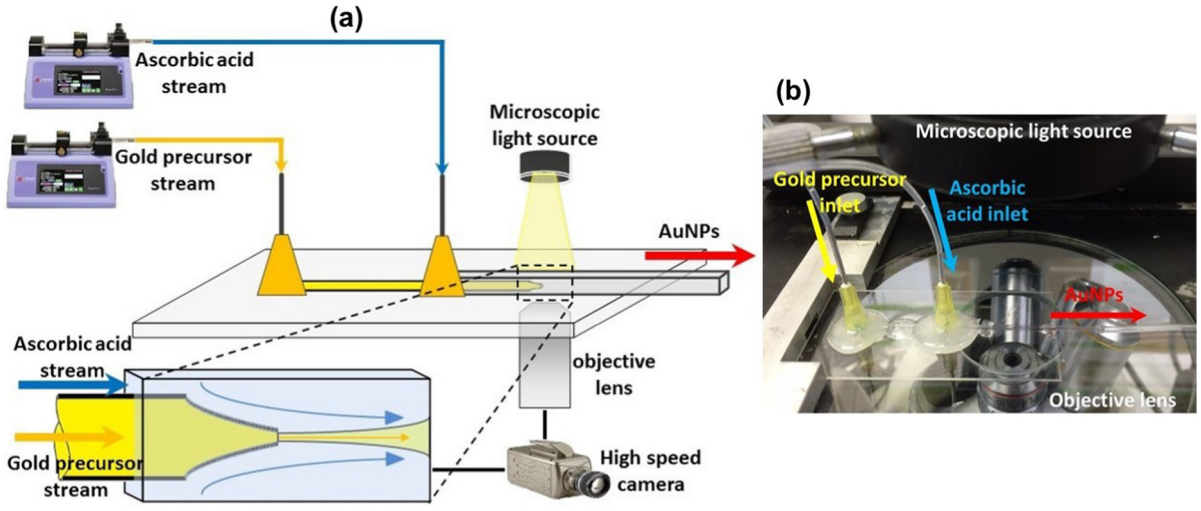

Fig. 1. (a) Schematic of the co-flow microfluidic experimental setup featuring the tapered orifice of round capillary inside the square capillary with the flow pattern of reactant streams (b) Photograph of the in-house made microfluidic device connected to reactant streams.

Table 1
Experimental conditions used in this work.

Orifice diameter, D_O (μm)	100, 180, 240
Flow rate of $HAuCl_4$ stream (ml/h)	15, 30, 60
Flow rate of ascorbic acid stream (ml/h)	15, 30, 60
pH of ascorbic acid solution	3.0 ± 0.3, 10.2 ± 0.3
Capping/stabilizing agent	1% (w/v) PVP K15 ($M_w \sim 10000$), PVP K30 ($M_w \sim 40000$), or PVP K90 ($M_w \sim 360000$)
Surface treatment methods	Hydrophobic surface treatment of the inner walls of the square capillary and the tip of the round capillary

2.3.3. Transmission electron microscopy

A JEOL 2000FX Transmission Electron Microscope (TEM) operated at an accelerating voltage of 200 kV was used to analyse the synthesised particles and to collect the selected area diffraction (SAD) patterns. Samples were prepared by placing a 10 μl drop of concentrated AuNPs suspension onto a graphene oxide layer on top of a holey carbon-coated copper grid (EM Resolutions Ltd, UK) and dried overnight.

2.3.4. X-ray powder diffraction analysis

The crystallinity of synthesised AuNPs were measured using the X-Ray powder diffraction (XRPD) diffractometer (Bruker Corporation, Billerica, MA, USA). Synthesised AuNPs suspensions were centrifuged using Hermle Z383 K (LabPlant, England), washed with deionised water and freeze dried using the Edwards Modulyo freeze dryer (Edwards High Vacuum, England) to obtain the dried AuNPs in powdered form.

3. Results and discussion

Two laminar reactant streams meet right after the injection capillary orifice (Fig. 1(a)). The diffusion of the reactants (ascorbic acid and auric chloride) takes place along the interface created between the two aqueous phases, followed by the chemical reaction:

$$2AuCl_4^- + 3C_6H_8O_6 \rightarrow 2Au^0 + 3C_6H_6O_6 + 8Cl^- + 6H^+ \quad (1)$$

3.1. Effect of the ascorbic acid stream flow rate and injection orifice diameter

Fig. 2(a) shows that smaller AuNPs can be synthesised by using smaller orifice diameters of the injection capillary and higher flow rates of ascorbic acid (AA) stream, while keeping the flow rate of $HAuCl_4$ solution constant at 15 ml/h.

This trend can be explained by the fact that an increased flow rate of ascorbic acid is likely to increase the diffusion rate of acid into the $HAuCl_4$ stream, due to the narrower flow pattern of the gold precursor stream, which in turn increases the likelihood of nucleation compared to growth of the NPs. Obtained results agree with the CNT and confirm that the nucleation dominates over growth at higher reaction rates (Thanh et al., 2014). Fig. 2(b) confirms that the PDI value increases with an increase of the ascorbic acid flow rate but no clear indication was shown in these experiments regarding the effect of the injection orifice diameter on the PDI of the synthesised AuNPs. According to DLS measurements, PDI lies between 0.05 (for an ideally monodispersed) and 0.7 (highly polydispersed) samples. In these experiments, the measured PDI values were between 0.1 and 0.4.

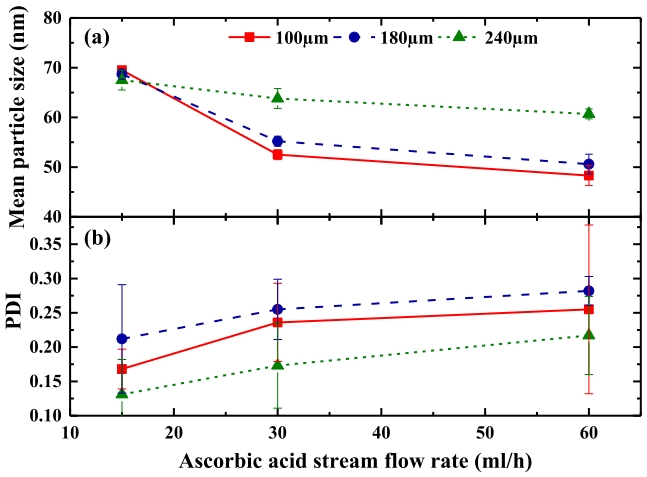

Fig. 2. The effect of the orifice diameter of the injection capillary and the flow rate of the ascorbic acid stream on: (a) the mean particle size; (b) the polydispersity index (DLS measurements). The flow rate of the gold precursor stream is 15 ml/h and the pH of the ascorbic acid stream is 10.2 ± 0.3. 1% (w/v) PVP K30 was used in the gold precursor stream as the stabiliser.

Fig. 3(a) shows that the absorbance peak amplitude of the synthesised AuNPs decreased with an increase of the flow rate of the ascorbic acid stream. This was due to the increased dilution of the NPs in the product stream at the higher flow rate of ascorbic acid. According to Fig. 3(b), when the flow rate ratio of the two streams was kept constant, smaller particles and higher particle concentrations were obtained at higher individual flow rates, as indicated by the highest maximum absorbance (1.72184 au) and the blueshift of the absorbance spectra indicating the smallest wavelength (550 nm) at the highest individual flow rates of 60 ml/h, which is in agreement with the previous findings showing that smaller particles indicate a higher absorbance and aggregated, bigger particles shows a lower absorbance (Alzoubi et al., 2015).

The results discussed above can be explained by the effect of the device geometry and fluid flow rates on rate of passive micro-mixing or molecular diffusion along the liquid/liquid interface due to laminar flow inside the collection capillary (Capretto et al., 2011). One of the key parameters that describes the passive micro-mixing is the average diffusion time t (s) of a molecule over a distance of x (m) which can be calculated by (Zhang et al., 2008):

$$t = \frac{x^2}{2D} \quad (2)$$

where D is the diffusion coefficient (m^2/s) of the molecule.

As indicated by Eq. (2), when the diffusion distance decreases, the diffusion time required decreases in proportion to the square power of x.

Fig. 4 illustrates how smaller orifice diameters generate narrower flow patterns with shorter diffusion distance, i.e. shorter residence time required for completion of reaction. In addition, when the total flow rate increases, the diffusion time decreases due to increase in the diffusion distance. As a result of the improved mixing, the process is dominated by nucleation, which in turn, generates smaller AuNPs. Conversely, large orifice diameters and low flow rates generate wider flow pattern which decreases the rate of diffusion, while increasing the residence time (Fig. 4(b)). As such, the process of particle formation is dominated by particle growth, and consequently, larger particles are produced. The results discussed above confirm that the AuNPs size can be controlled by changing the injection orifice diameter. In addition, smaller particles can be obtained by increasing the ascorbic acid flow rate, which is consistent with Long et co-workers' findings

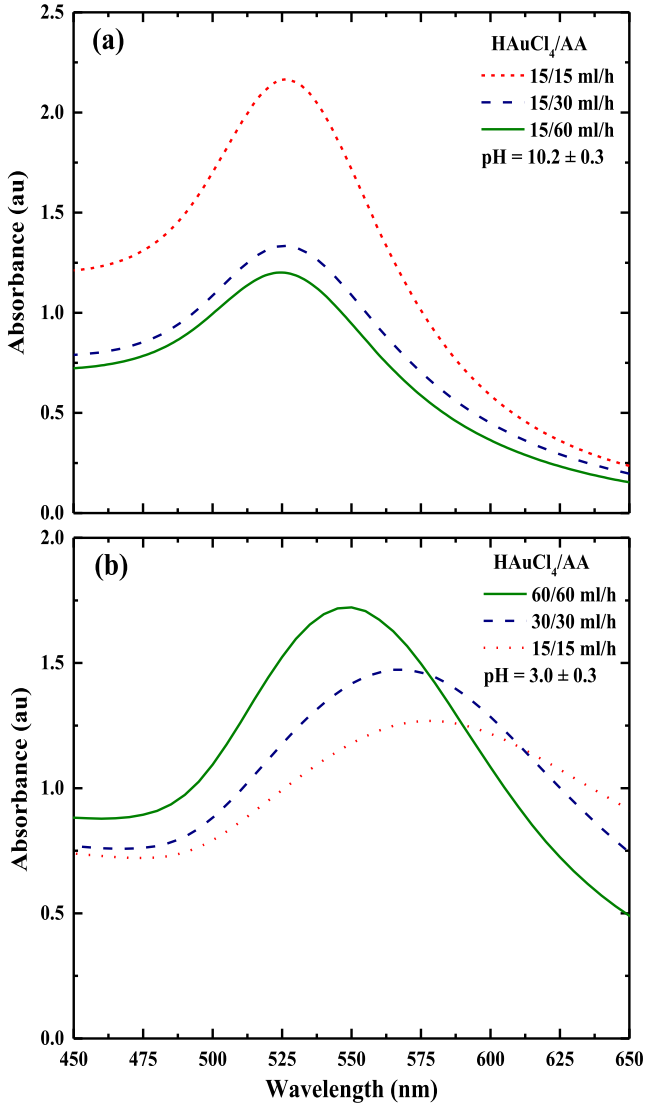

Fig. 3. (a) The effect of variable flow rate of the ascorbic acid stream (pH = 10.2 ± 0.3) on the absorbance spectra of AuNPs at D_O = 100 μm and the flow rate of the gold precursor stream of 15 ml/h; (b) The effect of variable flow rate of both streams on the absorbance spectra of AuNPs at D_O = 180 μm, the flow rate ratio of 1:1, and the pH of the ascorbic acid stream of 3. The D_P values: 47 nm at 60/60 ml/h, 70 nm at 30/30 ml/h, and 101 nm at 15/15 ml/h. The stabiliser was 1% (w/v) PVP K30.

showing that the synthesised particle size depends on the amount of reducing agent present (Long et al., 2009).

3.2. Effect of pH of ascorbic acid

Ascorbic acid is a weak acid with a low reducing power compared to other reducing agents commonly used to synthesise AuNPs, such as sodium borohydride ($NaBH_4$) and tri-sodium citrate ($Na_3C_6H_5O_7$). Due to its diprotic properties, ascorbic acid exists in three deprotonated spices with different reducing powers depending on the solution pH (Mukai et al., 1991), as illustrated by Eq. (3):

$$AsH_2 \overset{K_{a1}}{\Longleftrightarrow} AsH^- + H^+ \overset{K_{a2}}{\Longleftrightarrow} As^{2-} + 2H^+ \quad (3)$$

According to Tyagi et al. (2011), when the ascorbic acid pH is lower than 2, the synthesised AuNPs can aggregate in a short period of time. Taking into account this consideration, the pH of the ascorbic acid stream set in this work was 3.0 ± 0.3 or 10.2 ± 0.3.

Fig. 5 shows that when the pH of ascorbic acid solution was increased to approximately 10, the size of the synthesised particles decreased significantly which confirms that the ascorbic acid with higher pH possesses a higher reducing power than ascorbic acid with lower pH.

Table 2 shows that the polydispersity values were relatively low when the pH of ascorbic acid solution was maintained around 3. The aforementioned observations can be supported using the Alpha plot of the ascorbic acid which depicts the mole fraction of deprotonated ascorbate species vs pH (Luty-Błocho et al., 2013; Mukai et al., 1991). As shown in Eq. (3), ascorbic acid deprotonates into 3 different species of AsH_2, AsH^- and As^{2-} depending on the pH. H_2 dominates the solution at lower pH values up to 4, while the percentage of AsH^- increases to reach 100% when the pH is approximately 8. When the pH is 8, AsH_2 reaches its minimum concentration and exists in traces until pH 14. After pH 8, the percentage of AsH^- starts to decrease to reach 0% when the pH is 14. As^{2-} ions exist as a trace in the solution until the pH of 8, above which it starts to increase and reaches 100% when the pH is 14 (Mukai et al., 1991). As described above, when the pH is around 3, the solution is dominated by AsH_2, which has a weak reducing power due to the low pK_a value of 4.1. Hence, the redox reaction is slower, which leads to a reduced number of nucleation sites that makes particle growth more dominant resulting in larger particles with the lower PDI.

When the pH of the ascorbic acid solution is around 10, the solution is dominated by AsH^- species due to the higher pK_a (11.8). This species possesses relatively strong reducing power (Luty-Błocho et al., 2013) resulting in faster reaction and more nucleation sites, and consequently, higher nucleation, which slower growth and leads to higher PDI.

Fig. 5 also indicates that a blue-shift of the absorbance spectra, as indicated by absorbance peak position, takes place when the size of AuNPs decreases due to the change in the pH of the ascorbic acid solution. The same trend was obtained by Wagner et al. (2004), who observed that absorbance spectra of smaller AuNPs were blue-shifted. This effect is consistent with the colours of the nano-suspensions shown in Fig. 5 (inset).

Fig. 6 is consistent with the results in Figs. 2, 4, and 5 confirming that smaller orifice diameters produce smaller AuNPs. However, it proves that, the pH of the ascorbic acid solution affects more to synthesise smaller AuNPs than the injection orifice diameter.

Fig. 7 depicts XRPD and TEM SAD analysis confirming that AuNPs are semi-crystalline, which is consistent with most literature findings (Nagaraj et al., 2016). In addition, it is widely accepted that AuNP production follows the CNT as discussed above (Polte, 2015; Thanh et al., 2014).

3.3. Effect of capping/stabilizing agent

PVP is a biocompatible polymer extensively used in pharmaceutical, cosmetic and food products. PVP is amphiphilic due to the hydrophobic chain and highly hydrophilic pyrrolidone side chains which contain a C=O and a N (Heo et al., 2015). The interaction between PVP and gold surface is due to the donation of electrons from N or O in the side chain of the PVP (Koczkur et al., 2015).

PVP is used to provide long lasting stability to AuNPs and consequently longer product shelf life. Therefore, it is highly relevant to investigate the conditions at which optimal stabilisation is achieved. Here, we investigate the effect of PVP with different molecular weights on the size of the synthesised particles and their colloidal stability over 6 weeks period. To achieve the above, 5 ml of 1 mM $HAuCl_4$ solutions containing PVP K15 ($M_w \sim 10{,}000$), PVP K30 ($M_w \sim 40{,}000$) and PVP K90 ($M_w \sim 360{,}000$) at 1% (w/v) were prepared. The above solutions were reacted with 5 ml of 20 mM ascorbic acid solutions with the pH of 10.2 ± 0.3 under

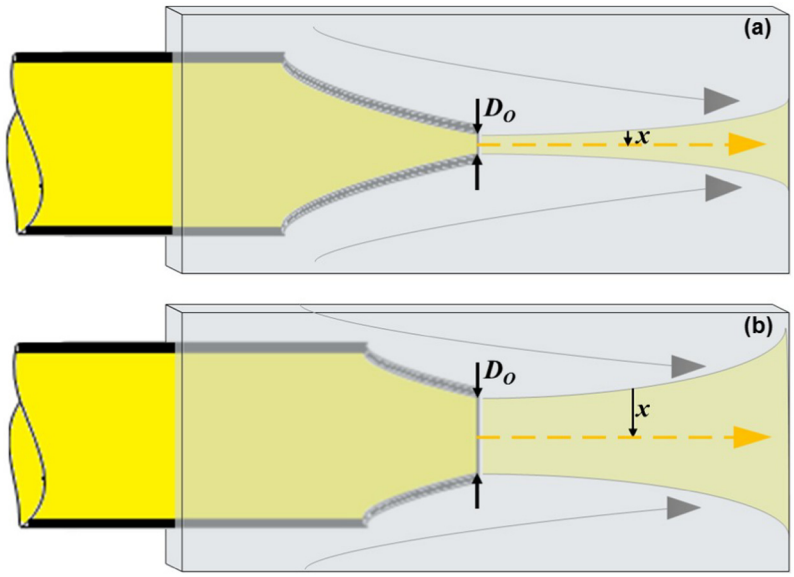

Fig. 4. The effect of the office diameter of the injection capillary on the flow pattern and the diffusion path length x along the interface for: (a) smaller D_O; (b) larger D_O.

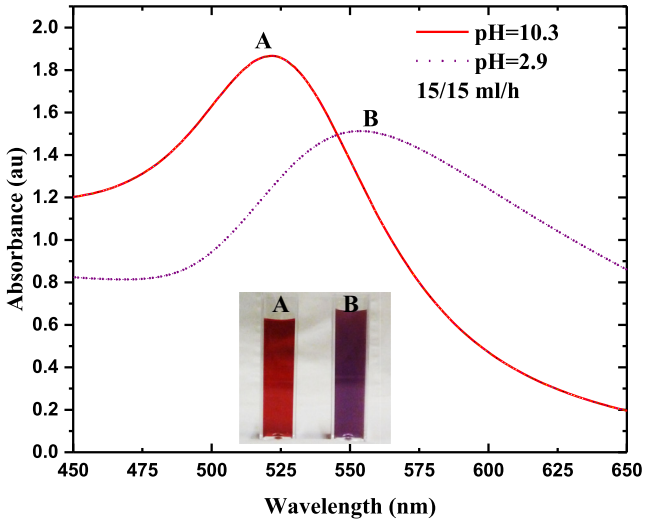

Fig. 5. Absorbance spectra of the AuNPs suspensions indicating the blueshift due to the decrease of particle size (inset - difference of the AuNPs suspension colour). D_O = 180 μm, the reactant stream flow rates ($HAuCl_4$/AA) were 15/15 ml/h. Stabilizing agent used was PVP K30. D_P of A is 59 nm and D_P of B is 135 nm. (For interpretation of the references to colour in this figure legend, the reader is referred to the web version of this article.)

Table 2
The PDI and average size of AuNPs according to DLS measurements, synthesised using ascorbic acid solution of different pH values when D_O = 180 μm. The reactant stream flow rates ($HAuCl_4$/AA) were 15/15 ml/h, the stabilizing agent used was PVP K30.

pH of ascorbic acid stream	10.2 ± 0.3	3.0 ± 0.3
PDI of AuNPs	0.170–0.365	0.036–0.135
Average particle size (nm)	59	114

room temperature and magnetic stirring for 15 min. The resulting AuNPs were characterised using DLS and UV–Vis spectroscopy on day 0 (right after the synthesis), after 3 days, then after week 1, 2, 3, 4, 5 and 6. Fig. 8 illustrates the TEM analyses carried out in day 0, week 2 and week 6. After week 6, due to visible agglomerates and precipitates observed in all samples, except in the nanosuspension containing PVP K30, the characterisation was abandoned for all samples and carried on only for the one containing PVP K30.

From Fig. 8 and Table 3, it is clear that PVP K90 yields larger AuNPs, according to both the DLS size measurements shown in Table 3 and TEM images, compared to PVP K30, PVP K15, or without capping agent. This trend is consistent throughout all the experimental results obtained. Polymers with higher molecular weights and longer chains promote bridging flocculation of the small particles due to loops, tails and trains extended to the solution from the particle surface resulting in large flocs (Adachi et al., 2012; Gregory and Barany, 2011; Otsubo, 1992). Kim et al. (2015) reported that flocculation and stabilization depends on the radius of gyration (R_g) and the concentration of the stabilizing agent in the medium. According to Fig. 8 and Table 3, it is clear that 1% (w/v) of PVP K90 is not the optimum concentration to stabilize the AuNPs, which is in line with Kim et al. (2015). On the other hand, Cao et al. (2000) reported that the radius of gyration of the PVP K15 chain may be too small to provide sufficient steric stabilization to smaller particles in long term. They also reported that moderate molecular weight range of PVP is better for stabilizing smaller particles which agrees with the findings of the experiments carried out in this paper proving that PVP K30 provides sufficient steric stabilization to AuNPs at a concentration of 1% (w/v).

The mean particle sizes obtained by the DLS were larger than those obtained from the TEM for all the experiments carried out. The DLS method measures the hydrodynamic diameter of the particles based on two main assumptions: (a) All particles are spherical and (b) the particles do not interact with each other. As a result, not only individual particles in the suspension are considered as spherical but also the clusters of particles. In addition, stabilizer layer and the solvent layer adsorbed onto the particle surface will be measured as one unit. The radius of gyration (R_g) of the stabilizing polymer depends on its molecular weight and chain length (Schwarz, 1990). R_g of PVP K15, PVP K30 and PVP K90 was found to be 2 nm, 4 nm, and 12 nm respectively (Schwarz, 1990). McFarlane et al. (2010) calculated R_g for PVP K30 and PVP K90 using static light scattering and reported the values of 15 ± 1 nm and 38 ± 1 nm respectively. Therefore, AuNPs stabilized with a higher molecular weight PVP, such as PVP K90, should show larger particle diameters in DLS compared to the TEM measurements.

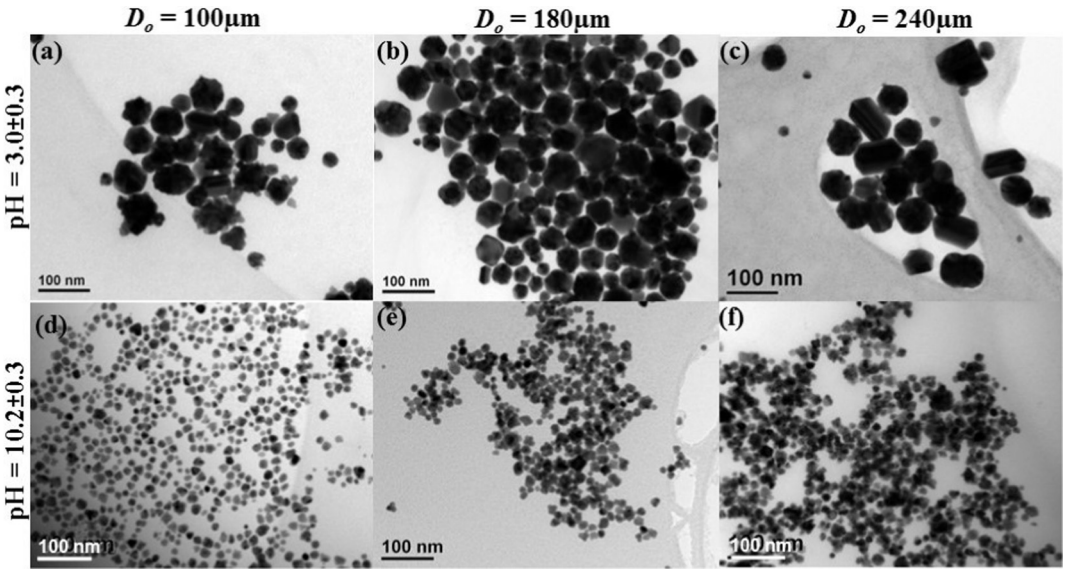

Fig. 6. TEM images of AuNPs synthesised using different injection orifice diameters (D_O) and using ascorbic acid streams of different pH. The reactant flow rates were 15/60 ml/h ($HAuCl_4$/AA). PVP K30 was used as the stabilizer. The TEM particle sizes are: (a) (48 ± 17) nm; (b) (90 ± 36) nm; (c) (66 ± 5) nm; (d) (13 ± 3) nm; (e) (16 ± 11) nm; (f) (15 ± 7) nm.

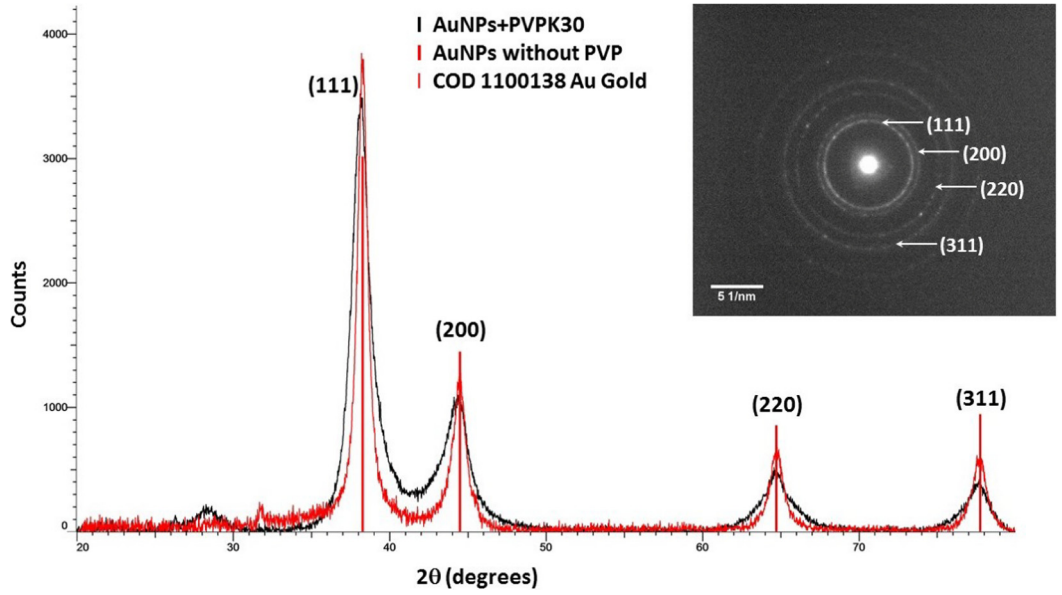

Fig. 7. XRPD profile of the synthesised AuNPs matches with the Au standard Bragg reflections (111), (200), (220) and (311) of the Face Centred Cubic (FCC) lattice structure from the Crystallography Open Database (data sheet 1100138). Inset: TEM SAD pattern matched with the Bragg reflections from the XRPD measurements.

To further investigate the outcome of the four different stabilization scenarios, the UV–Vis absorbance spectra are depicted in Fig. 9. The UV–Vis spectra depicted in Fig. 9(a) show that AuNPs suspension without stabilizing agent changed significantly over the 6 weeks period. The visual observations of the samples (Fig. 10) were consistent with Fig. 9(a) as the glass vial walls turned to purple while the suspension colour changed from purple to faded purple over 6 weeks. Fig. 9(b) and (d) indicate a slight decrease of the absorbance over 6 weeks. Fig. 9 confirms these outcomes as the sample colour changes from darker to lighter shade over the 6 weeks period. Flocs and precipitates were observed over time in all sample vials except the suspension stabilized with PVP K30 which is consistent with the decrease of absorbance peak amplitude and the faded colour shown in Figs. 9(a), (b), (d) and 10. Figs. 9(c) and 10 confirm that AuNPs stabilized with 1% (w/v) PVP K30 are the most stable over the 6 weeks period.

Surface plasmon of NPs depends not only on the size, shape and type of the particles but also on the properties of the surrounding environment (Kreibig and Vollmer, 1995) and the distance between NPs (Petryayeva and Krull, 2011). Depending on the dielectric constant and the refractive index of the surrounding solution, λ_{max} of the suspension changes (Kooyman and Kooyman, 2008; Tudos et al., 2008). Therefore, the observed changes in the absorbance spectra during the storage were not only due to a change in the particle size but also due to changes in the solution concentration (due to precipitates) and the changes of the particle surface properties (reconformation of polymer loops, trains and tails on particle surfaces) (Adachi et al., 2012). As such, the absorbance spectra cannot be used alone for AuNPs characterisation unless the particles have been suspended in deionized water after synthesis. Nevertheless, by comparing the absorbance peaks from UV–Vis spectra with the DLS measure-

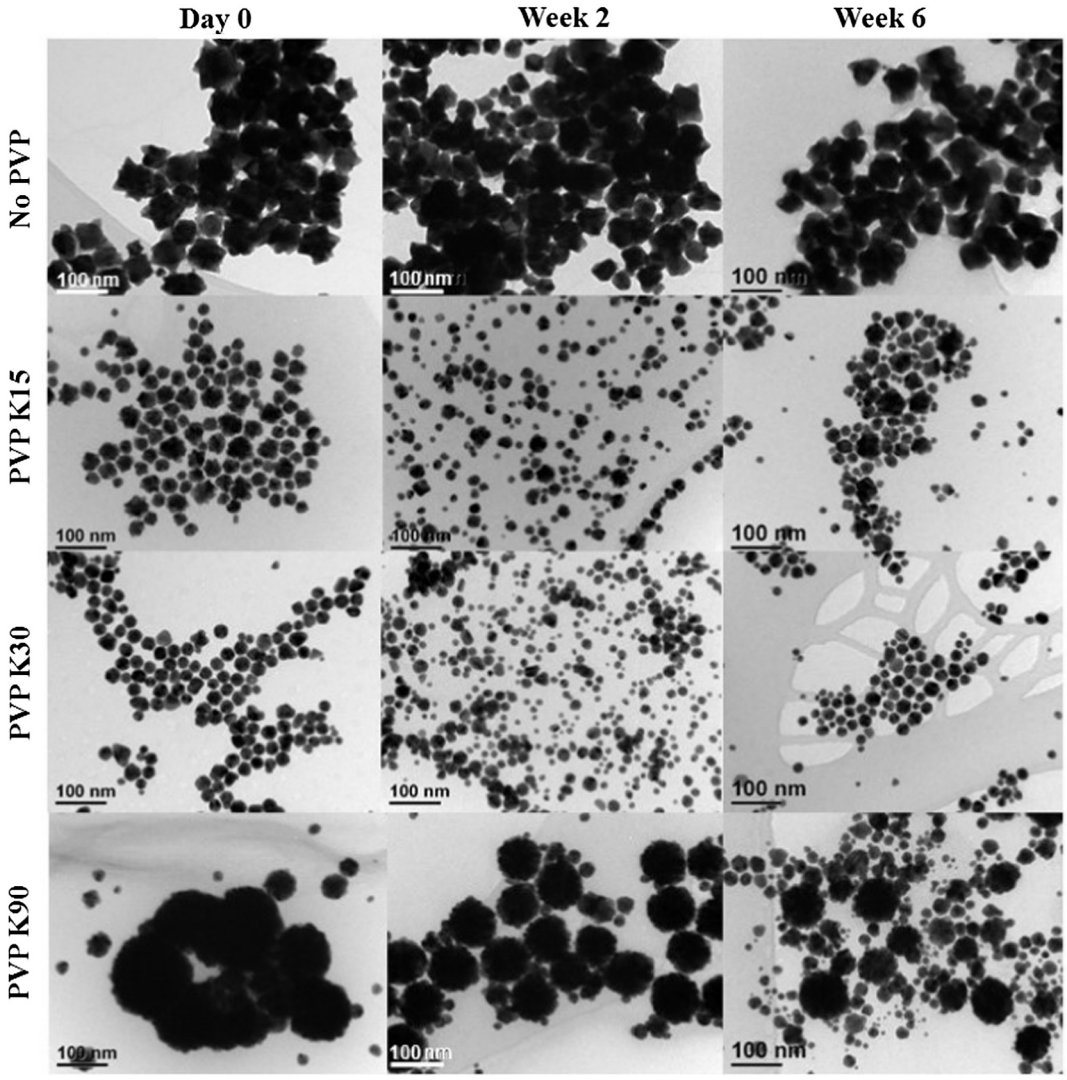

Fig. 8. TEM micrographs of AuNPs capped using 1% (w/v) PVP in $HAuCl_4$ solution over 6 weeks. Scale bar is 100 nm (particle size measurements are in Table 3). 5 ml of 1 mM $HAuCl_4$ solutions containing 1% (w/v) relevant PVP was reacted with 5 ml of 20 mM ascorbic acid solutions with pH of 10.2 ± 0.3 under room temperature by magnetic stirring for approximately 15 mins.

Table 3
DLS particle size measurement and TEM image particle size measurements of AuNPs illustrated in Fig. 8. The concentration of PVP is 1% (w/v) in $HAuCl_4$ solution.

	Day 0	Week 2	Week 6
No PVP	DLS: 65 nm TEM: (66 ± 5) nm	DLS: 77 nm TEM: (52 ± 14) nm	DLS: 87 nm TEM: (52 ± 13) nm
PVP K15	DLS: 56 nm TEM: (27 ± 11) nm	DLS: 59 nm TEM: (17 ± 7) nm	DLS: 62 nm TEM: (23 ± 8) nm
PVP K30	DLS: 83 nm TEM: (22 ± 5) nm	DLS: 72 nm TEM: (19 ± 6) nm	DLS: 92 nm TEM: (20 ± 7) nm
PVP K90	DLS: 299 nm TEM: (69 ± 47) nm	DLS: 227 nm TEM: (61 ± 18) nm	DLS: 182 nm TEM: (24 ± 14) nm

ments and the TEM images, more reliable conclusions can be made regarding the change of the NPs sizes.

4. Reactor fouling mitigation

Fouling is one of the major limitations associated with microfluidic devices. To mitigate or prevent reactor fouling, different approaches such as treating the capillary inner wall with a hydrophobic solution, increasing the pH of ascorbic acid stream and using PVP as the capping agent were investigated. Further details can be found in the supplementary materials.

4.1. Surface treatment of the square capillary and pH

The hydrophobization of the inner walls of the reactor through silanization can create high slip boundary conditions which reduce wetting and enhance shear rate that suppresses fouling (Rothstein, 2010). When the pH of ascorbic acid was maintained at 3, more than 95% of the available ascorbic acid was fully protonated to a weaker reducing ascorbate (AsH^-) species (Mukai et al., 1991). This species adsorbed onto the NP surface to provide relatively small negative charge to the particles. As a consequence, the resulting repulsive forces between the NPs were not sufficient to overcome attractive Van der Waal's forces, in which case, the NPs tended to agglomerate. Similarly, if the slip boundary conditions are not sufficient, the repulsive electrostatic forces between the particle surface and the reactor wall will result in the fouling as a consequence of adsorption of particles onto the reactor walls (Fig. S2). Conversely, when the pH of ascorbic acid was maintained at 10, stronger As^{2-} ions with higher negative charges were formed on the particles, which enhances their stability in suspension resulting in minimum reactor fouling (Fig. S3).

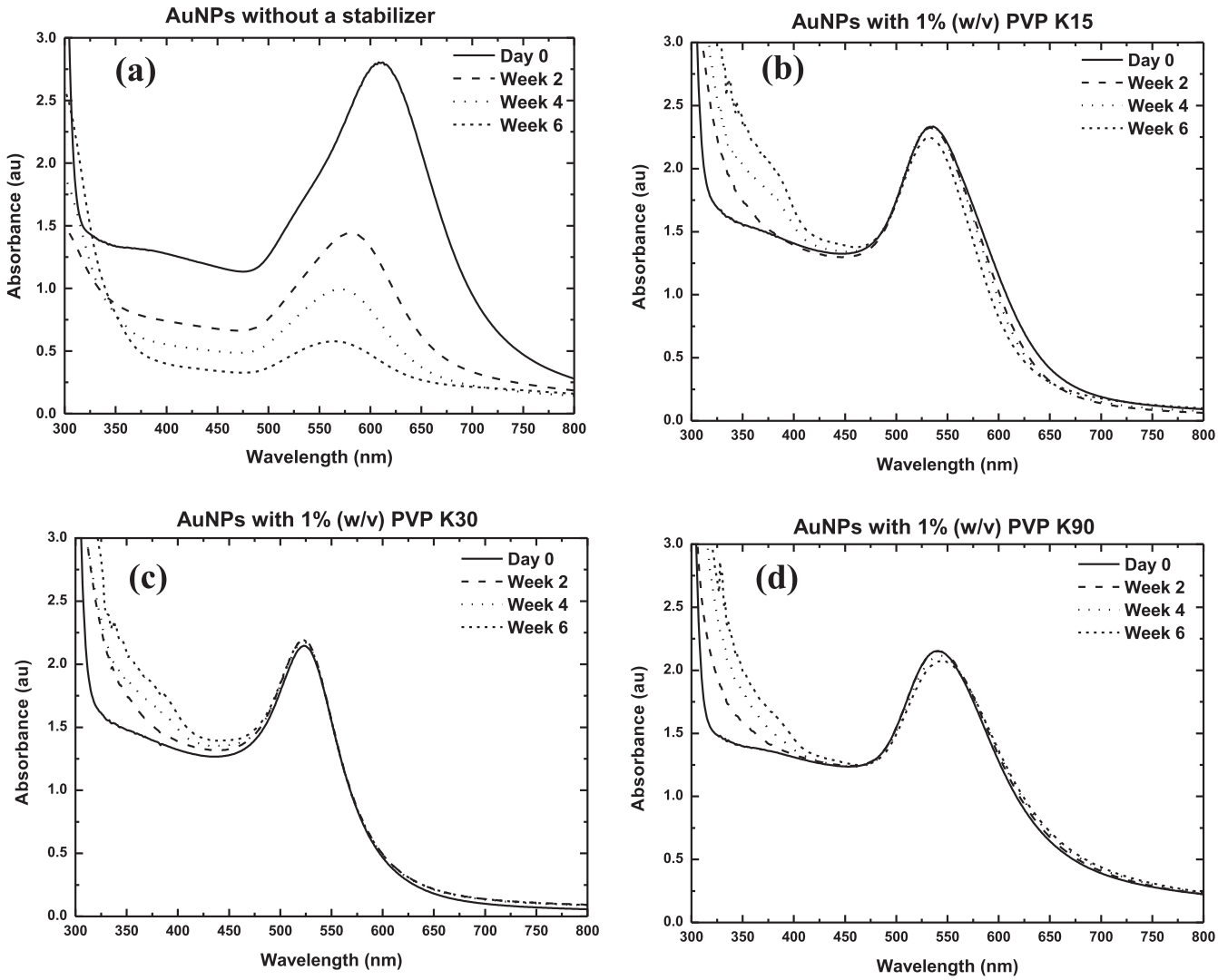

Fig. 9. Absorbance spectra of AuNPs stabilized with 1% (w/v) PVP with different molecular weights synthesised with 1 mM $HAuCl_4$ solution and 20 mM ascorbic acid solution with a pH of 10.2 ± 0.3.

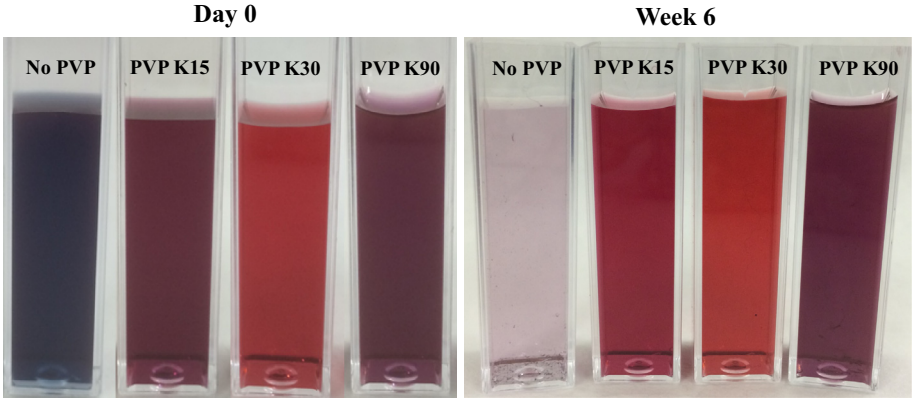

Fig. 10. Colour of AuNPs in suspension without a stabilizer and stabilized with PVP K15, PVP K30 and PVP K90 respectively over 6-week time period.

4.2. Use of PVP and ascorbic acid solution with a higher pH

The walls of the borosilicate glass reactor used in this work have an isoelectric point between 2.1 and 2.8 (Hunter et al., 2013; Lameiras et al., 2008). As such, the reactor walls become negatively charged at pH values greater than the isoelectric point, and the negative charge increases with an increased pH. In addition, since Au(0) has zero charge, the charge of AuNPs suspended in aqueous media strongly depends on the chemical species adsorbed onto the particle surface.

As reported in the literature, AuNPs stabilized with mercapto-succinic acid presented an isoelectric point between 4.9 and 5.5,

while AuNPs capped with 4-carboxythiophenol showed an isoelectric point between 7.3 and 7.8 (Gole et al., 1999). Citrate stabilized AuNPs aggregate quickly when pH is reduced to 1.7 due to the protonation of citrate ions (previously adsorbed on the NP surface) leaving the nanoparticles without a citrate cap which will be affected by Van der Waal's forces resulting in agglomeration (Lee et al., 2001).

For the experiments carried out without PVP, the only available chemical species that adsorb on the AuNPs are the ascorbate ions. Operating at pH = 10 (with pK_a at 11.8) ensures that there is a high concentration of deprotonated ascorbic acid anions available, which provides a large negative charge on the NPs. Therefore, increased pH should ensure the repulsion of the particles from the reactor surface, which minimizes the reactor fouling. As expected, the rate of fouling was reduced when the pH of the incoming aqueous ascorbic acid stream was increased to 10, compared to the instance where no fouling control methods were in place (Figs. S1 and S3). However, since pH strongly affects particle size, it will be impossible to employ ascorbic acid with higher pH to mitigate reactor fouling in the case of synthesizing larger particles.

The use of PVP as a capping/stabilizing agent was also investigated to minimize the reactor fouling particularly when combined with the increased pH of ascorbic acid solution (Fig. S4). As expected and reported in the literature, the PVP layer formed around the AuNPs makes them more stable and hydrophilic, which in turn reduces their deposition on reactor walls (Heo et al., 2015).

5. Conclusions

A two-phase microfluidic process for facile continuous production of PVP stabilized spherical AuNPs with controlled size has been developed. To optimize the process and produce AuNPs with a targeted particle size and PDI, the effect of the injection orifice diameter, reactant flow rates, pH of ascorbic acid stream and the molecular weight of the capping agent were systematically investigated. Smaller injection orifices generated narrower jet of the gold precursor solutions, which decreased the diffusion distance and increased efficiency of mixing leading to more nucleation and consequently to smaller AuNPs. Higher ascorbic acid flow rates increased the dilution effect. As consequence, the synthesis process was dominated by the nucleation which resulted in smaller particles. Ascorbic acid solutions at higher pH possess a stronger reducing power due to its dibasic properties which led to smaller AuNPs. It was also observed that the PDI of the synthesized particles was not affected by the injection orifice diameter. However lower PDI can be achieved when the pH of the ascorbic acid solution was maintained at around 3, along with a lower flow rate of the ascorbic acid stream. Further to above results XRPD/TEM SAD analysis confirmed that AuNPs synthesized in these experiments were in a semi crystalline FCC lattice structure.

The stability of the synthesized AuNPs was investigated over 6 weeks in order to determine the PVP molecular weight that provides the most effective long lasting stabilization. PVP K30, used at 1% (w/v), turned out to be the most effective stabilizing agent. It is worth noting that the PDI was not significantly affected by the difference in the PVP molecular weight. As the ascorbic acid and PVP are some of the most biocompatible reagents, the AuNPs synthesized in these experiments can be used for drug delivery applications which will be the scope of the authors' future work.

To mitigate reactor fouling, three different approaches were investigated. Treating the inner walls of the square capillary with OTMS reduced their wettability and consequently reduced the deposition of AuNPs. Using ascorbic acid solutions with higher pH increased the negative charges at the surface of the synthesized particles increasing wall repulsion and consequently reducing fouling significantly. PVP adsorbed onto the AuNP surface provides an enhanced steric stability to the NPs, which mitigated their deposition on the reactor walls. The combination of the above three methods helped to prevent reactor fouling significantly. To further mitigate the reactor fouling and provide-long term operation, the development of a liquid hydrophobic barrier between the reaction and the reactor walls seems to be the most effective way. To undertake this investigation, a droplet-based three phase glass capillary microfluidic device will be used in the future work as well as designing a new glass capillary holder to explore possibilities for a scale up.

Acknowledgements

The authors would like to thank Dr. Zhaoxia Zhou and Dr. Keith Yendall from the Loughborough Materials Characterization Centre (LMCC), Loughborough University, UK for their assistance in the TEM imaging and XRPD measurements.

Appendix A. Supplementary material

Supplementary data associated with this article can be found, in the online version, at http://dx.doi.org/10.1016/j.ces.2017.05.035.

References

Adachi, Y., Kobayashi, A., Kobayashi, M., 2012. Structure of colloidal flocs in relation to the dynamic properties of unstable suspension. Int. J. Polym. Sci. 2012, 1–14. http://dx.doi.org/10.1155/2012/574878.

Alzoubi, F.Y., Alzouby, J.Y., Alqadi, M.K., Alshboul, H.A., Aljarrah, K.M., 2015. Synthesis and characterization of colloidal gold nanoparticles controlled by the pH and ionic strength. Chinese J. Phys. 53, 100801–100809. http://dx.doi.org/10.6122/CJP.20150601E.

Bouras, N., Madjoubi, Ma., Kolli, M., Benterki, S., Hamidouche, M., 2009. Thermal and mechanical characterization of borosilicate glass. Phys. Procedia 2, 1135–1140. http://dx.doi.org/10.1016/j.phpro.2009.11.074.

Cao, K., Li, B.-F., Huang, Y., Li, B.-G., Pan, Z.-R., 2000. Mechanism and model of dispersion polymerization using homopolymer as dispersant in polar media. Macromol. Symp. 150, 187–194. http://dx.doi.org/10.1002/1521-3900(200002)150:1 187::AID-MASY187 3.0.CO;2-M.

Capretto, L., Zhang, X., Cheng, W., Hill, M., 2011. Micromixing within microfluidic devices, microfluidics. Springer-Verlag, Berlin Heidelberg.. http://dx.doi.org/10.1007/128_2011_150.

Chandran, S.P., Chaudhary, M., Pasricha, R., Ahmad, A., Sastry, M., 2006. Synthesis of gold nanotriangles and silver nanoparticles using Aloe vera plant extract. Biotechnol. Prog. 22, 577–583. http://dx.doi.org/10.1021/bp0501423.

Conde, J., Doria, G., Baptista, P., 2012. Noble metal nanoparticles applications in cancer. J. Drug Deliv. 2012, 1–12. http://dx.doi.org/10.1155/2012/751075.

Duraiswamy, S., Khan, Sa., 2009. Droplet-based microfluidic synthesis of anisotropic metal nanocrystals. Small 5, 2828–2834. http://dx.doi.org/10.1002/smll.200901453.

Ekanem, E.E., Nabavi, S.A., Vladisavljevic, G.T., Gu, S., 2015. Structured biodegradable polymeric microparticles for drug delivery produced using flow focusing glass microfluidic devices. ACS Appl. Mater. Interfaces 7, 23132–23143. http://dx.doi.org/10.1021/acsami.5b06943.

Gao, Y., Hu, Y., Li, C., Zhao, X., Huang, X., Liu, R., 2014. Kiwifruit as reducing reagent for green synthesis of gold nanoparticles at room temperature. Nanosci. Nanotechnol. Lett. 6, 118–123. http://dx.doi.org/10.1166/nnl.2014.1733.

Gole, A.M., Sathivel, C., Lachke, A., Sastry, M., 1999. Size separation of colloidal nanoparticles using a miniscale isoelectric focusing technique. J. Chromatogr. A 848, 485–490. http://dx.doi.org/10.1016/S0021-9673(99)00408-2.

Gomez, L., Sebastian, V., Irusta, S., Ibarra, A., Arruebo, M., Santamaria, J., 2014. Scaled-up production of plasmonic nanoparticles using microfluidics: from metal precursors to functionalized and sterilized nanoparticles. Lab. Chip. 14, 325–332. http://dx.doi.org/10.1039/c3lc50999k.

Gómez-de Pedro, S., Puyol, M., Alonso-Chamarro, J., 2010. Continuous flow synthesis of nanoparticles using ceramic microfluidic devices. Nanotechnology 21, 1–6. http://dx.doi.org/10.1088/0957-4484/21/41/415603.

Gregory, J., Barany, S., 2011. Adsorption and flocculation by polymers and polymer mixtures. Adv. Colloid Interface Sci. 169, 1–12. http://dx.doi.org/10.1016/j.cis.2011.06.004.

Heider, P.L., Born, S.C., Basak, S., Benyahia, B., Lakerveld, R., Zhang, H., Hogan, R., Buchbinder, L., Wolfe, A., Mascia, S., Evans, J.M.B., Jamison, T.F., Jensen, K.F., 2014. Development of a multi-step synthesis and workup sequence for an integrated, continuous manufacturing process of a pharmaceutical. Org. Process Res. Dev. 18, 402–409. http://dx.doi.org/10.1021/op400294z.

Heo, J.H., Kim, K.Il., Cho, H.H., Lee, J.W., Lee, B.S., Yoon, S., Park, K.J., Lee, S., Kim, J., Whang, D., Lee, J.H., 2015. Ultrastable-stealth large gold nanoparticles with DNA directed biological functionality. Langmuir 31, 13773–13782. http://dx.doi.org/10.1021/acs.langmuir.5b03534.

Horikoshi, S., Serpone, N., 2013. Chapter 1: introduction to nanoparticles. In: Microwaves in Nanoparticle Synthesis: Fundamentals and Applications. John Wiley & Sons, pp. 1–24. http://dx.doi.org/10.1002/9783527648122.

Hunter, R.J., Ottewill, R.H., Rowell, R.L., 2013. Zeta Potential in Colloid Science: Principles and Applications. Elsevier Science.

Johnston, I.D., McCluskey, D.K., Tan, C.K.L., Tracey, M.C., 2014. Mechanical characterization of bulk Sylgard 184 for microfluidics and microengineering. J. Micromech. Microeng. 24, 1–7. http://dx.doi.org/10.1088/0960-1317/24/3/035017.

Jun, H., Fabienne, T., Florent, M., Coulon, P.E., Nicolas, M., Olivier, S., 2012. Understanding of the size control of biocompatible gold nanoparticles in millifluidic channels. Langmuir 28, 15966–15974. http://dx.doi.org/10.1021/la303439f.

Kim, S., Hyun, K., Moon, J.Y., Clasen, C., Ahn, K.H., 2015. Depletion stabilization in nanoparticle-polymer suspensions: Multi-length-scale analysis of microstructure. Langmuir 31, 1892–1900. http://dx.doi.org/10.1021/la504578x.

Koczkur, K.M., Mourdikoudis, S., Polavarapu, L., Skrabalak, S.E., 2015. Polyvinylpyrrolidone (PVP) in nanoparticle synthesis. Dalt. Trans. 44, 17883–17905. http://dx.doi.org/10.1039/C5DT02964C.

Kooyman, R.P.H., Kooyman, R.P.H., 2008. Chapter 2. Physics of Surface Plasmon Resonance. In: Handbook of Surface Plasmon Resonance. Royal Society of Chemistry, Cambridge, pp. 15–34. http://dx.doi.org/10.1039/9781847558220.

Kreibig, U., Vollmer, M., 1995. Chapter 2 & Chapter 4. In: Optical Properties of Metal Clusters, Springer Series in Materials Science. Springer, Berlin Heidelberg, Berlin, Heidelberg, pp. 187–193, 328–333. http://dx.doi.org/10.1007/978-3-662-09109-8.

Lameiras, F.S., Souza, A leles de, de Melo, V.A.R., martins Nunes, E.H., Braga, I.D., 2008. Measurement of the zeta potential of planar surfaces with a rotating disk. Mater. Res. 11, 217–219. http://dx.doi.org/10.1590/S1516-14392008000200018.

Laouini, A., Koutroumanis, K.P., Charcosset, C., Georgiadou, S., Fessi, H., Holdich, R.G., Vladisavljević, G.T., 2013. PH-sensitive micelles for targeted drug delivery prepared using a novel membrane contactor method. ACS Appl. Mater. Interfaces 5, 8939–8947. http://dx.doi.org/10.1021/am4018237.

Lazarus, L.L., Riche, C.T., Marin, B.C., Gupta, M., Malmstadt, N., Brutchey, R.L., 2012. Two-phase microfluidic droplet flows of ionic liquids for the synthesis of gold and silver nanoparticles. ACS Appl. Mater. Interfaces 4, 3077–3083. http://dx.doi.org/10.1021/am3004413.

Lee, H.C., Gaensslen, R.E., Ramotowski, R., 2001. Chapter 13: Fingermark detection using nanoparticles. In: Advances in Fingerprint Technology - third ed., pp. 319–326. http://dx.doi.org/10.1007/s13398-014-0173-7.2.

Lee, J.-S., 2010. Recent progress in gold nanoparticle-based non-volatile memory devices. Gold Bull. 43, 189–199. http://dx.doi.org/10.1007/BF03214986.

Long, N.N., Van Vu, L., Kiem, C.D., Doanh, S.C., Nguyet, C.T., Hang, P.T., Thien, N.D., Quynh, L.M., 2009. Synthesis and optical properties of colloidal gold nanoparticles. J. Phys. Conf. Ser. 187, 1–8. http://dx.doi.org/10.1088/1742-6596/187/1/012026.

Luty-Błocho, M., Pacławski, K., Wojnicki, M., Fitzner, K., 2013. The kinetics of redox reaction of gold(III) chloride complex ions with L-ascorbic acid. Inorganica Chim. Acta 395, 189–196. http://dx.doi.org/10.1016/j.ica.2012.10.031.

Mascia, S., Heider, P.L., Zhang, H., Lakerveld, R., Benyahia, B., Barton, P.I., Braatz, R.D., Cooney, C.L., Evans, J.M.B., Jamison, T.F., Jensen, K.F., Myerson, A.S., Trout, B.L., 2013. End-to-end continuous manufacturing of pharmaceuticals: Integrated synthesis, purification, and final dosage formation. Angew. Chemie - Int. Ed. 52, 12359–12363. http://dx.doi.org/10.1002/anie.201305429.

McFarlane, N.L., Wagner, N.J., Kaler, E.W., Lynch, M.L., 2010. Poly(ethylene oxide) (PEO) and poly(vinyl pyrolidone) (PVP) induce different changes in the colloid stability of nanoparticles. Langmuir 26, 13823–13830. http://dx.doi.org/10.1021/la101907s.

Mukai, K., Nishimura, M., Kikuchi, S., 1991. Stopped-flow investigation of the reaction of vitamin C with tocopheroxyl radical in aqueous Triton X-100 micellar solutions. J. Biol. Chem. 266, 274–278.

Nabavi, S.A., Vladisavljević, G.T., Gu, S., Ekanem, E.E., 2015. Double emulsion production in glass capillary microfluidic device: Parametric investigation of droplet generation behaviour. Chem. Eng. Sci. 130, 183–196. http://dx.doi.org/10.1016/j.ces.2015.03.004.

Nagaraj, S.K., Shivanna, S., Subramani, N.K., 2016. Revisiting powder X-ray diffraction technique: a powerful tool to characterize polymers and their composite films. J. Mater. Sci. 4, 1–5. http://dx.doi.org/10.4172/2321-6212.1000158.

Nune, S.K., Chanda, N., Shukla, R., Katti, K., Kulkarni, R.R., Thilakavathy, S., Mekapothula, S., Kannan, R., Katti, K.V., 2009. Green nanotechnology from tea: phytochemicals in tea as building blocks for production of biocompatible gold nanoparticles. J. Mater. Chem. 19, 2912–2920. http://dx.doi.org/10.1039/b822015h.

Odetade, D.F., Vladisavljevi, G.T., 2016. Microfluidic fabrication of hydrocortisone nanocrystals coated with polymeric stabilisers. Micromachines 7, 1–20. http://dx.doi.org/10.3390/mi7120236.

Othman, R., Vladisavljević, G.T., Bandulasena, H.C.H., Nagy, Z.K., 2015a. Production of polymeric nanoparticles by micromixing in a co-flow microfluidic glass capillary device. Chem. Eng. J. 280, 316–329. http://dx.doi.org/10.1016/j.cej.2015.05.083.

Othman, R., Vladisavljević, G.T., Nagy, Z.K., 2015b. Preparation of biodegradable polymeric nanoparticles for pharmaceutical applications using glass capillary microfluidics. Chem. Eng. Sci. 137, 119–130. http://dx.doi.org/10.1016/j.ces.2015.06.025.

Otsubo, Y., 1992. Effect of particle size on the bridging structure and elastic properties of flocculated suspensions. J. Colloid Interface Sci. 153, 584–586. http://dx.doi.org/10.1016/0021-9797(92)90350-U.

Perks, B., 2010. Gold fever. Chem. World, 48–50.

Petryayeva, E., Krull, U.J., 2011. Localized surface plasmon resonance: Nanostructures, bioassays and biosensing-A review. Anal. Chim. Acta 706, 8–24. http://dx.doi.org/10.1016/j.aca.2011.08.020.

Pissuwan, D., Niidome, T., Cortie, M.B., 2011. The forthcoming applications of gold nanoparticles in drug and gene delivery systems. J. Control. Release 149, 65–71. http://dx.doi.org/10.1016/j.jconrel.2009.12.006.

Polte, J., 2015. Fundamental growth principles of colloidal metal nanoparticles – a new perspective. CrystEngComm 17, 6809–6830. http://dx.doi.org/10.1039/c5ce01014d.

Qureshi, Z.S., Sarawade, P.B., Hussain, I., Zhu, H., Al-Johani, H., Anjum, D.H., Hedhili, M.N., Maity, N., D'Elia, V., Basset, J.M., 2016. Gold nanoparticles supported on fibrous silica nanospheres (KCC-1) as efficient heterogeneous catalysts for CO oxidation. ChemCatChem, 1671–1678. http://dx.doi.org/10.1002/cctc.201600106.

Rajeshkumar, S., Malarkodi, C., Gnanajobitha, G., Paulkumar, K., Vanaja, M., Kannan, C., Annadurai, G., 2013. Seaweed-mediated synthesis of gold nanoparticles using Turbinaria conoides and its characterization. J. Nanostructure Chem. 3, 1–7. http://dx.doi.org/10.1186/2193-8865-3-44.

Roduner, E., 2006. Size matters: why nanomaterials are different. Chem. Soc. Rev. 35, 583–592. http://dx.doi.org/10.1039/b502142c.

Rothstein, J.P., 2010. Slip on superhydrophobic surfaces. Annu. Rev. Fluid Mech. 42, 89–109. http://dx.doi.org/10.1146/annurev-fluid-121108-14555.

Schwarz, W., 1990. Pvp: A Critical Review of the Kinetics and Toxicology of Polyvinylpyrrolidone (Povidone). CRC Press.

Spivak, M.Y., Bubnov, R.V., Yemets, I.M., Lazarenko, L.M., Tymoshok, N.O., Ulberg, Z. R., 2013. Gold nanoparticles - the theranostic challenge for PPPM: nanocardiology application. EPMA J. 4, 1–18. http://dx.doi.org/10.1186/1878-5085-4-18.

Sugano, K., Uchida, Y., Ichihashi, O., Yamada, H., Tsuchiya, T., Tabata, O., 2010. Mixing speed-controlled gold nanoparticle synthesis with pulsed mixing microfluidic system. Microfluid. Nanofluidics 9, 1165–1174. http://dx.doi.org/10.1007/s10404-010-0637-9.

Thanh, N.T.K., Maclean, N., Mahiddine, S., 2014. Mechanisms of nucleation and growth of nanoparticles in solution. Chem. Rev. 114, 7610–7630. http://dx.doi.org/10.1021/cr400544s.

Tudos, A.J., Schasfoort, R.B.M., Tudos, A.J., Schasfoort, R.B.M., 2008. Chapter 1. Introduction to surface plasmon resonance. In: Handbook of Surface Plasmon Resonance. Royal Society of Chemistry, Cambridge, pp. 1–14.

Turkevich, J., Stevenson, P.C., Hillier, J., 1951. A study of the nucleation and growth processes in the synthesis of colloidal gold. Discuss. Faraday Soc. 11, 55–75. http://dx.doi.org/10.1039/DF9511100055.

Tyagi, H., Kushwaha, A., Kumar, A., Aslam, M., 2011. PH-dependent synthesis of stabilized gold nanoparticles using ascorbic acid. Int. J. Nanosci. 10, 857–860. http://dx.doi.org/10.1142/S0219581X11009301.

Verma, H.N., Singh, P., Chavan, R.M., 2014. Gold nanoparticle: synthesis and characterization. Vet. World 7, 72–77. http://dx.doi.org/10.14202/vetworld.2014.72-77.

Verma, M.S., Rogowski, J.L., Jones, L., Gu, F.X., 2015. Colorimetric biosensing of pathogens using gold nanoparticles. Biotechnol. Adv. 33, 666–680. http://dx.doi.org/10.1016/j.biotechadv.2015.03.003.

Vladisavljević, G.T., Laouini, A., Charcosset, C., Fessi, H., Bandulasena, H.C.H., Holdich, R.G., 2014a. Production of liposomes using microengineered membrane and co-flow microfluidic device. Colloids Surfaces A Physicochem. Eng. Asp. 458, 168–177. http://dx.doi.org/10.1016/j.colsurfa.2014.03.016.

Vladisavljević, G.T., Shahmohamadi, H., Das, D.B., Ekanem, E.E., Tauanov, Z., Sharma, L., 2014b. Glass capillary microfluidics for production of monodispersed poly (dl-lactic acid) and polycaprolactone microparticles: Experiments and numerical simulations. J. Colloid Interface Sci. 418, 163–170. http://dx.doi.org/10.1016/j.jcis.2013.12.002.

Wagner, J., Kirner, T., Mayer, G., Albert, J., Köhler, J., 2004. Generation of metal nanoparticles in a microchannel reactor. Chem. Eng. J. 101, 251–260. http://dx.doi.org/10.1016/j.cej.2003.11.021.

Wagner, J., Kohler, J.M., 2005. Continuous synthesis of gold nanoparticles in a microreactor. Nano Lett. 5, 685–691. http://dx.doi.org/10.1021/nl050097t.

Zhang, Z., Zhao, P., Xiao, G., Lin, M., Cao, X., 2008. Focusing-enhanced mixing in microfluidic channels. Biomicrofluidics 2, 1–9. http://dx.doi.org/10.1063/1.2894313.

Zhao, C.-X., He, L., Qiao, S.Z., Middelberg, A.P.J., 2011. Nanoparticle synthesis in microreactors. Chem. Eng. Sci. 66, 1463–1479. http://dx.doi.org/10.1016/j.ces.2010.08.039.